

# Fabrication of uniform $\text{SnO}_2\text{-SiO}_2\text{-Pt}$ composite nanofibres via co-electrospinning

Yu-Jin Lee, Hyo-Jin Ahn\*

*Department of Materials Science & Engineering, Seoul National University of Science and Technology, Seoul 139-743, Republic of Korea*

Received 14 September 2012; received in revised form 10 December 2012; accepted 10 December 2012

Available online 26 December 2012

## Abstract

We successfully fabricated uniform  $\text{SnO}_2\text{-SiO}_2\text{-Pt}$  composite nanofibres (NFs) by using a co-electrospinning technique, in which we set up two coaxial capillaries. Morphology control of NFs was investigated, along with their structural properties and chemical compositions. Furthermore, to systematically investigate the morphological changes in  $\text{SnO}_2\text{-SiO}_2\text{-Pt}$  composite NFs, the relative weight ratios of the Sn precursor to the Si precursor including the 4 wt% Pt precursor were controlled at 3:1, 1:1, and 1:3. To demonstrate the formation mechanism of the composite NFs, the precursor positions of the shell section and the core section in co-electrospinning were reversed. The resultant composite NFs were investigated by using X-ray diffraction (XRD), scanning electron microscopy (SEM), transmission electron microscopy (TEM) with energy dispersive X-ray spectroscopy (EDS), and X-ray photoelectron spectroscopy (XPS). These results showed that in the case of the optimum weight ratio (1:1) of the Sn precursor in the shell section to the Si precursor including the 4 wt% Pt precursor in the core section,  $\text{SnO}_2$  and Pt nanoparticles were uniformly grown on  $\text{SiO}_2$  NFs, implying the successful formation of uniform  $\text{SnO}_2\text{-SiO}_2\text{-Pt}$  composite NFs.

© 2012 Elsevier Ltd and Techna Group S.r.l. All rights reserved.

**Keywords:** A. Calcination; B1. Fibers; B2. Nanocomposites; E. Structural applications

## 1. Introduction

One-dimensional (1-D) nanofibres (NFs), which have peculiar optical, electrical, chemical, and electrochemical properties, have gained considerable attention recently for their potential use in many applications such as optics, electronics, biondiagnostics, and energy conversion [1–3]. Several studies have attempted to synthesize various 1-D NFs. In particular, many types of NFs with different morphologies, such as composite, core-shell, hollow, rods, and belts, have been synthesized hitherto [3]. Among the various morphologies of NFs, 1-D composite NFs have received considerable attention because of their useful and unique properties, along with complementary properties in NFs. Thus far, various synthetic methods, such as hydrothermal method, template-directed electrochemical method, chemical bath deposition, and electrospinning, have been proposed for the fabrication of 1-D composite

NFs [4–7]. Among the above-mentioned methods, electrospinning, which has important advantages such as simplicity, low-cost, and mass producibility, is one of the most useful methods for the fabrication of 1-D composite NFs. Previous researchers have mainly studied composite NFs composed of two different phases fabricated using an electrospinning method. For example, Jeong et al. fabricated the  $\text{Co}_3\text{O}_4\text{-RuO}_2$  composite NFs via electrospinning and demonstrated their structural properties by performing X-ray diffraction (XRD), X-ray photoelectron spectroscopy (XPS), and transmission electron microscopy (TEM) [8]. Zhao et al. fabricated porous  $\text{CuO/SnO}_2$  composite NFs via electrospinning for use in  $\text{H}_2\text{S}$  sensing [9]. Wang et al. fabricated  $\text{C/Fe}_3\text{O}_4$  composite NFs for use as anode materials in lithium-ion batteries and demonstrated enhanced reversible capacity and good rate capability [10]. Thus, until now, researchers have mainly studied fabrication of composite NFs composed of two phases using an electrospinning method. However, fabrication and morphology control of composite NFs composed of three different phases using a co-electrospinning technique have not yet

\*Corresponding author. Tel.: +82 2 970 6622; fax: +82 2 973 6657.

E-mail address: [hjahn@seoultech.ac.kr](mailto:hjahn@seoultech.ac.kr) (H.-J. Ahn).

been realized. Therefore, in this study, we successfully synthesized  $\text{SnO}_2\text{-SiO}_2\text{-Pt}$  composite NFs via co-electrospinning and performed morphology control in order to obtain uniform composite NFs. These uniform  $\text{SnO}_2\text{-SiO}_2\text{-Pt}$  composite NFs could be utilized in various applications such as Li-ion batteries, electrochemical capacitors, and sensors.

## 2. Preparation

### 2.1. Experimental

In order to fabricate composite NFs consisting of three different phases, a co-electrospinning technique, divided by the core-section and shell-section, was employed, as shown in Fig. 1. To confirm the morphological changes in the composite NFs, the relative weight ratios of the Sn precursor to the Si precursor were controlled at 3:1, 1:1, and 1:3 to give samples A, B, and C, respectively. In all the samples, 4 wt% of the Pt precursor was equally added to the Si precursor. In the core section, tetraethylorthosilicate (TEOS, Aldrich) as the Si precursor and chloroplatinic acid hydrate ( $\text{H}_2\text{PtCl}_6 \cdot x\text{H}_2\text{O}$ , Aldrich) as the Pt precursor were dissolved in N,N-dimethylformamide (DMF, Aldrich), and polyvinylpyrrolidone (PVP,  $M_w=1,300,000$  g/mol, Aldrich) as a stabilizer was stirred into the above-dissolved solution for 2 h at room temperature. In the shell section, tin (II) chloride dihydrate ( $\text{SnCl}_2$ , Aldrich) as the Sn precursor dissolved in N,N-dimethylformamide (DMF, Aldrich) was mixed with polyvinylpyrrolidone (PVP,  $M_w=1,300,000$  g/mol, Aldrich) for 2 h at room temperature. The two coaxial capillaries consist of two parts; one is a 26-gauge inner capillary for the Si and Pt precursors, and the other is an 18-gauge outer capillary for the Sn

precursor, as shown in Fig. 1(a). In addition, the precursor position of the shell section and the core section was reversed in order to investigate the formation mechanism of composite NFs, as shown in Fig. 1(b). This will be discussed later in the results and discussion section. The feeding rates during co-electrospinning were fixed at 0.01 ml/h for the core section and 0.02 ml/h for the shell section. The voltage was maintained at  $\sim 18$  kV for all the samples. The resulting as-spun NFs were heat-treated at  $300^\circ\text{C}$  for 2 h in air and then calcined at  $500^\circ\text{C}$  for 5 h. Thus, uniform  $\text{SnO}_2\text{-SiO}_2\text{-Pt}$  composite NFs were successfully fabricated.

### 2.2. Characterization

The crystallinity and structural properties of the fabricated NFs were characterized by using an X-ray diffractometer (Rigaku Rint 2500) equipped with  $\text{Cu K}_\alpha$  radiation. The morphology and composition of all the samples were examined by using a field-emission scanning electron microscope (Hitachi S-4700) and a transmission electron microscope (JEOL 2100F, KBSI Suncheon Center) with energy-dispersive X-ray spectroscopy (EDS). The chemical bonding states of all the samples were examined using an X-ray photoelectron spectroscope (ESCALAB 250) equipped with an  $\text{Al K}_\alpha$  X-ray source.

## 3. Results and discussion

Fig. 2 shows XRD data obtained from samples A, B, and C after calcination. The main characteristic diffraction peaks for the  $\text{SnO}_2$  phases were observed at  $2\theta = \sim 26.6^\circ$ ,  $33.8^\circ$ ,  $37.9^\circ$ , and  $51.7^\circ$ , corresponding to the (110), (101), (200), and (211) planes, respectively, of the tetragonal

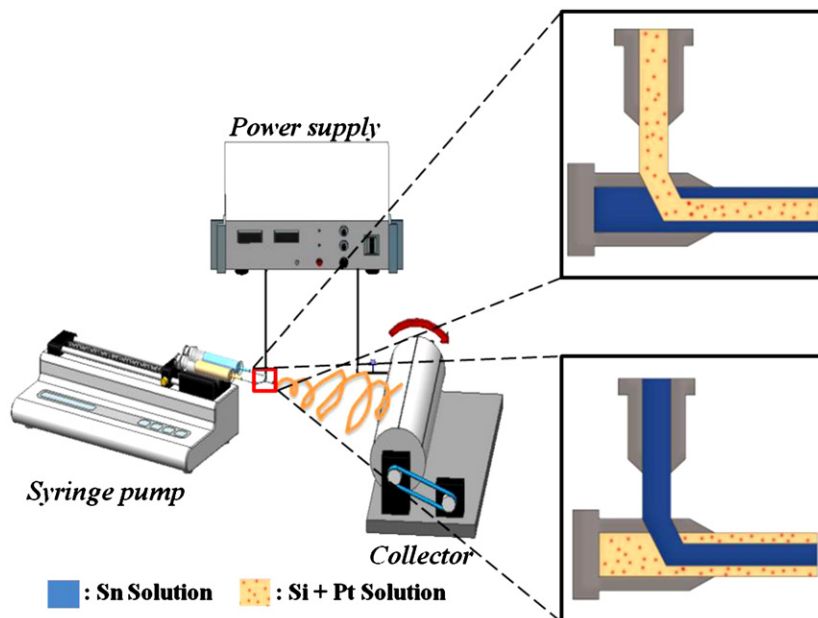


Fig. 1. Schematic of two coaxial capillaries in a co-electrospinning apparatus.

rutile structure of  $\text{SnO}_2$  (space group  $P4_2/mnm$  [136]; JCPDS card no. 41–1445). Further, the main characteristic diffraction peaks for the Pt phases were observed at  $2\theta = \sim 39.7^\circ$  and  $46.2^\circ$ , corresponding to crystalline Pt phases having face-centered cubic structure (space group  $Fm3m$  [225]; JCPDS card no. 04–0802). No diffraction peak related to the  $\text{SiO}_2$  phases was observed for any of the samples, thus indicating amorphous characteristics. In particular, no diffraction peak shift for  $\text{SnO}_2$  and  $\text{SiO}_2$  was observed, signifying the existence of composite phases. Thus, the XRD results showed that composite NFs were

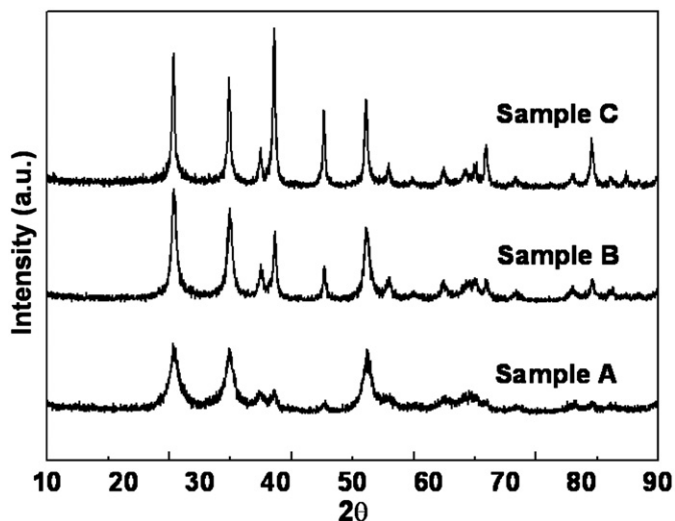


Fig. 2. XRD plots obtained from samples A, B, and C after calcination.

composed of crystalline  $\text{SnO}_2$  phases, amorphous  $\text{SiO}_2$  phases, and crystalline Pt phases.

Fig. 3 shows the FESEM images for samples A, B, and C before calcination ((a)–(c)) and after calcination ((d)–(f)). The as-spun samples consist of the core section formed by the Si precursor–PVP composite and the Pt precursor–PVP composite and the shell section formed by the Sn precursor–PVP composite. The diameter of the as-spun samples before calcination was in the range of  $\sim 180$ – $230$  nm. The diameters of samples A, B, and C after calcination are  $\sim 70$ – $100$  nm,  $\sim 100$ – $130$  nm, and  $\sim 100$ – $170$  nm, respectively. As seen in Fig. 3(d), sample A exhibits small aggregation of  $\text{SnO}_2$  nanophases on the  $\text{SiO}_2$  NFs because it had a higher loading amount of  $\text{SnO}_2$ . Sample B (Fig. 3(e)) exhibits uniform dispersion of  $\text{SnO}_2$  nanophases on the Si NFs. Sample C (Fig. 3(f)) exhibits relatively larger aggregations of  $\text{SnO}_2$  nanophases on the Si NFs because it had a lower loading amount of  $\text{SnO}_2$ . Therefore, uniform composite NFs having three different phases were formed when the weight ratio of the Sn precursor to the Si precursor was 1:1.

Fig. 4 shows the TEM images obtained from samples A, B, and C after calcination. Samples A and B consist of relatively dark, large nanoparticles related to the  $\text{SnO}_2$  phases; relatively darker, small nanoparticles related to the Pt phases; and relatively light NFs related to the  $\text{SiO}_2$  phases. As shown in Fig. 4(b), sample B exhibits uniform morphology (e.g. grain size and distribution of the  $\text{SnO}_2$  phases) of the composite NFs compared to sample A. In particular, as shown in Fig. 4(c), sample C exhibits non-uniform composite NFs having three different phases, i.e.

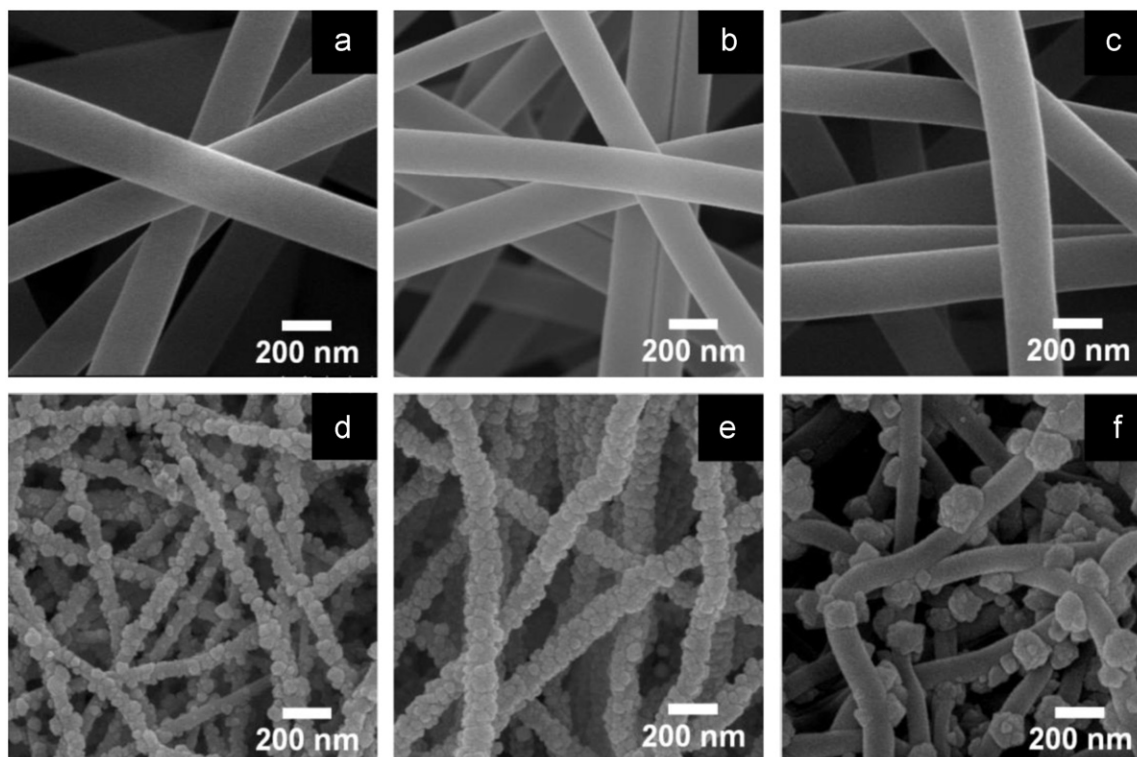


Fig. 3. FESEM images of samples A, B, and C before calcination ((a)–(c)) and after calcination ((d)–(f)).

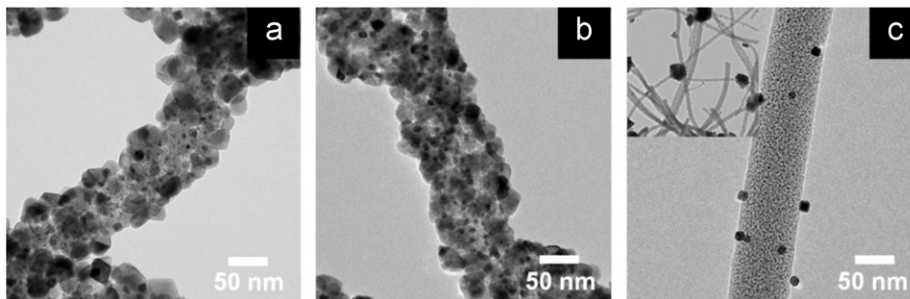


Fig. 4. TEM images of samples A, B, and C after calcination ((a)–(c)).

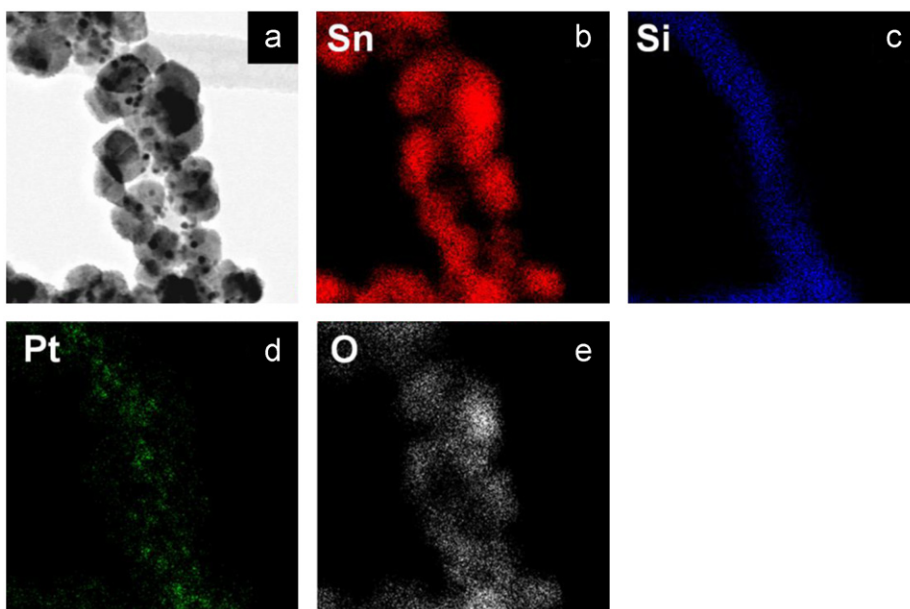


Fig. 5. TEM-EDS mapping data obtained from sample A.

it consists of relatively dark Pt nanoparticles composited on and within the relatively light  $\text{SiO}_2$  NFs and the larger  $\text{SnO}_2$  aggregation (see the upper-left inset). Therefore, the TEM results indicated that sample B, fabricated via co-electrospinning, consisted of uniform  $\text{SnO}_2$ – $\text{SiO}_2$ –Pt composite NFs having three different phases.

To clearly investigate the distributed composition of the Sn, Si, and Pt atoms in the composite NFs, TEM-EDS mapping of sample A was performed, as shown in Fig. 5(a)–(e). The EDS mapping data indicate that Sn atoms form relatively large grains on the NFs, Si atoms form uniform nanoparticles in the 1-D NFs, and Pt atoms form both relatively large grains ( $\text{SnO}_2$  phases) and uniform NFs ( $\text{SiO}_2$  phases). These results imply that the composite NFs having three different phases are composed of uniformly distributed  $\text{SnO}_2$  nanophases grown on the  $\text{SiO}_2$  NFs, along with Pt nanophases distributed within the  $\text{SnO}_2$  and  $\text{SiO}_2$  phases.

To further investigate the chemical bonding states and composition of elemental Sn, Si, and Pt, XPS analyses were carried out. Fig. 6(a)–(i) shows the XPS spectra of the Sn  $3d$ , Si  $2p$ , and

Pt  $4d$  core levels obtained from samples A, B, and C. The XPS spectra for the Sn  $3d_{5/2}$  and  $3d_{3/2}$  photoelectrons of all the samples were observed at  $\sim 486.6$  and  $\sim 495.0$  eV, which implies that elemental Sn was formed in the  $\text{SnO}_2$  phases. The XPS spectra for the Si  $2p$  photoelectrons of all the samples were observed at  $\sim 103.2$  eV, indicating that elemental Si was formed in the  $\text{SiO}_2$  phases [11]. In addition, the XPS spectra for the Pt  $4d_{5/2}$  and  $4d_{3/2}$  photoelectrons of all the samples were observed at  $\sim 316.5$  and  $\sim 333.2$  eV, implying the formation of the metallic Pt phases. Thus, the XPS results reveal that Sn, Si, and Pt in all the samples exist as Sn (IV), Si (IV), and Pt (0) states, corresponding to  $\text{SnO}_2$ ,  $\text{SiO}_2$ , and metallic Pt phases, respectively. The XRD, FESEM, TEM with EDS mapping, and XPS analyses confirm that uniform  $\text{SnO}_2$ – $\text{SiO}_2$ –Pt composite NFs were successfully synthesized via a co-electrospinning technique.

To further investigate the formation mechanism of the uniform composite NFs (sample B), we changed the position of the precursor solutions relative to the core section and the shell section during co-electrospinning,

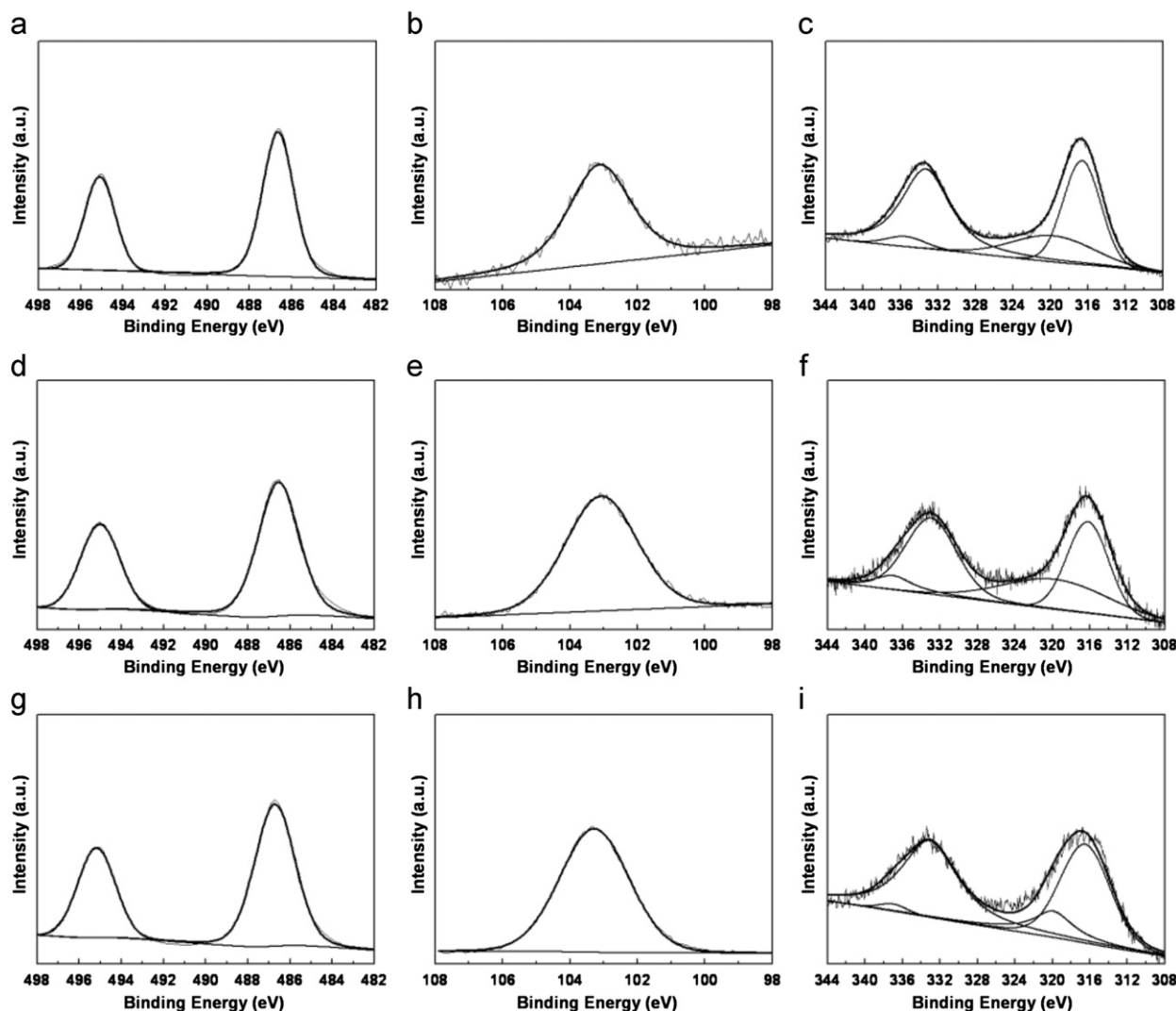


Fig. 6. XPS spectra of the Sn 3d, Si 2p, and Pt 4d core levels for sample A ((a)–(c)), sample B ((d)–(f)), and sample C ((g)–(i)).

from that shown in Fig. 1(a) to that shown in Fig. 1(b). Interestingly, we confirmed morphology changes similar to those seen in sample C, which are indicative of non-uniform composite NFs, as shown in Fig. 7(a). Thus, the formation mechanism for uniform composite NFs could be attributed to the position of the precursor solutions in co-electrospinning. The Si and Pt precursor solutions were placed in the core section, and the Sn precursor solution was placed in the shell section (Fig. 7(b)). After calcination, the SnO<sub>2</sub> nanoparticles were uniformly formed on the SiO<sub>2</sub> NFs (Fig. 3(e)). This is because the Sn precursor in the shell section reacted directly with the oxygen source in the air during calcination. However, when the Sn precursor solution was placed in the core section and the Si and Pt precursor solutions were placed in the shell section (Fig. 7(c)), after calcination, a large aggregation of the SnO<sub>2</sub> nanoparticles was distributed on the SiO<sub>2</sub> NFs (Fig. 7(a)). In this case, the Sn atoms in the core section moved into the shell section and the Si atoms in the shell section moved into the core section during calcination

because Sn atoms tend to oxidize preferentially compared to Si atoms. Thus, Sn atoms moved by diffusion from the core section to the shell section to combine with oxygen in the air during calcinations, then causing the aggregation of Sn atoms. Therefore, in order to synthesize uniform SnO<sub>2</sub>–SiO<sub>2</sub>–Pt composite NFs having three different phases, it is very important to adjust the position of the precursors and select an optimum weight ratio of the Sn precursor to the Si precursor.

#### 4. Conclusions

Uniform SnO<sub>2</sub>–SiO<sub>2</sub>–Pt composite NFs were successfully synthesized via co-electrospinning. Their morphology control and structural properties were demonstrated by XRD, FESEM, TEM, TEM–EDS mapping, and XPS analyses. The uniform composite NFs could be obtained by a combination of using the optimum weight ratio (1:1) of the Sn precursor to the Si precursor and adjusting the position of the precursors related to the Sn precursor in the

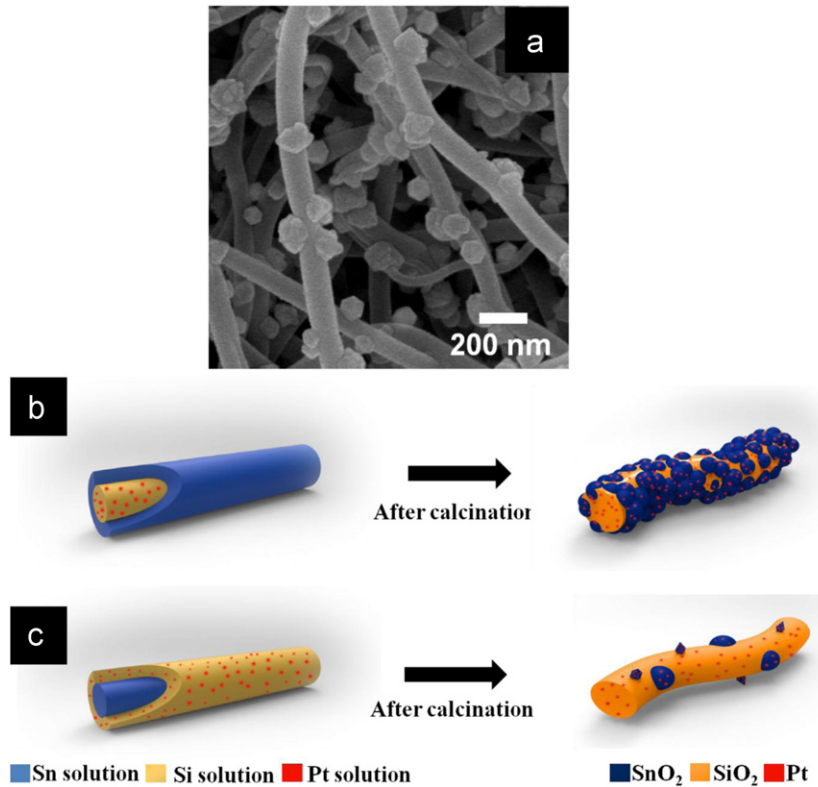


Fig. 7. SEM image of non-uniform composite NFs obtained from an experimental method of Fig. 1(b). (a). Schematic of uniform composite NFs (b) and non-uniform composite NFs (c) depending on the position of the precursor solutions in co-electrospinning.

shell section and the Si–Pt precursor in the core section. The  $\text{SnO}_2$  nanophases were uniformly distributed on the  $\text{SiO}_2$  NFs together with the Pt nanophases formed within  $\text{SnO}_2$  nanophases and  $\text{SiO}_2$  NFs. Thus, co-electrospinning could be considered a powerful technique for fabricating uniform  $\text{SnO}_2$ – $\text{SiO}_2$ –Pt composite NFs having three different phases.

### Acknowledgment

This research was supported by Basic Science Research Program through the National Research Foundation of Korea (NRF) funded by the Ministry of Education, Science and Technology (2012-007444).

### References

- [1] S. Park, J.H. Lim, S.W. Chung, C.A. Mirkin, Self-assembly of mesoscopic metal–polymer amphiphiles, *Science* 303 (2004) 348–351.
- [2] Y. Xia, P. Yang, Y. Sun, Y. Wu, B. Mayers, B. Gates, Y. Yin, F. Kim, H. Yan, One-dimensional nanostructures: synthesis, characterization, and applications, *Advanced Materials* 15 (2003) 353–389.
- [3] G.H. An, S.Y. Jeong, T.Y. Seong, H.J. Ahn, One-pot fabrication of hollow  $\text{SiO}_2$  nanowires via an electrospinning technique, *Materials Letters* 65 (2011) 2377–2380.
- [4] J.X. Wang, X.W. Sun, Y. Yang, K.K.A. Kyaw, X.Y. Huang, J.Z. Yin, J. Wei, H.V. Demir, Free-standing ZnO–CuO composite nanowires array films and their gas sensing properties, *Nanotechnology* 22 (2011) 325704.
- [5] J. Wang, J. Dai, T. Yarlagadda, Carbon nanotube-conducting polymer composite nanowires, *Langmuir* 21 (2005) 9–12.
- [6] Y. Shen, J.I. Hong, S. Xu, S. Lin, H. Fang, S. Zhang, Y. Ding, R.L. Snyder, Z.L. Wang, A general approach for fabricating arch-shaped composite nanowires arrays by pulsed laser deposition, *Advanced Functional Materials* 20 (2010) 703–707.
- [7] J.B. Lee., S.Y. Jeong, W.J. Moon, T.Y. Seong, H.J. Ahn, Preparation and characterization of electro-spun  $\text{RuO}_2$ – $\text{Ag}_2\text{O}$  composite nanowires for electrochemical capacitors, *Journal of Alloys and Compounds* 509 (2011) 4336–4340.
- [8] S.Y. Jeong, H.J. Ahn, T.Y. Seong, Synthesis and characterization of  $\text{Co}_3\text{O}_4$ / $\text{RuO}_2$  composite nanofibers fabricated by an electrospinning method, *Materials Letters* 65 (2011) 471–473.
- [9] Y. Zhao, X. He, J. Li, X. Cao, J. Jia, Porous  $\text{CuO}/\text{SnO}_2$  composite nanofibers fabricated by electrospinning and their  $\text{H}_2\text{S}$  sensing properties, *Sensors and Actuators B* 165 (2012) 82–87.
- [10] L. Wang, Y. Yu, P.C. Chen, D.W. Zhang, C.H. Chen, Electrospinning synthesis of  $\text{C}/\text{Fe}_3\text{O}_4$  composite nanofibers and their application for high performance lithium-ion batteries, *Journal of Power Sources* 183 (2008) 717–723.
- [11] J.F. Moulder, W.F. Stickle, P.E. Sobol, K.D. Bomben, *Handbook of X-ray Photoelectron Spectroscopy*, Physical Electronics, Physical Electronics, Inc., Eden Prairie, Minnesota, 1995.